Applied Catalysis B: Environmental 99 (2010) 127–134

Contents lists available at ScienceDirect

Applied Catalysis B: Environmental

journal homepage: www.elsevier.com/locate/apcatb

Application of VO_x/Al_2O_3 and $Fe_2(MoO_4)_3$–MoO_3 catalysts for the selective reaction and detection of ethanol in multi-component hydrocarbon fuel mixtures

Joseph E. Gatt, Hari Nair, Chelsey D. Baertsch*

School of Chemical Engineering, Purdue University, West Lafayette, IN 47907, USA

ARTICLE INFO

Article history:
Received 11 January 2010
Received in revised form 2 June 2010
Accepted 4 June 2010
Available online 12 June 2010

Keywords:
Microsensor selectivity
Ethanol
Iron molybdate
Vanadium oxide
Fuel sensor

ABSTRACT

This work presents for the first time the development of a selective catalyst to enable selective hydrocarbon detection when coupled with a microcalorimetric sensor. Specifically, the application of VO_x/Al_2O_3 and $Fe_2(MoO_4)_3$–MoO_3 catalysts as selective sensor substrates for thermal microsensor detection of ethanol in automotive fuel is described. At 453 K, $8VO_x/Al_2O_3$ (monolayer surface density of ~8 V/nm^2) and $Fe_2(MoO_4)_3$–MoO_3 (Mo:Fe = 1.9) catalysts convert ethanol towards one highly exothermic oxidative dehydrogenation product, acetaldehyde, with selectivities of 95% and 98%, respectively. For $8VO_x/Al_2O_3$ and $Fe_2(MoO_4)_3$–MoO_3, rates at 453 K are 1.3×10^{-6} and 3.4×10^{-6} mol ethanol converted/g s, respectively, and they are independent of ethanol concentration from 0.2 to 2.0 kPa ethanol. At 453 K, these catalysts provide excellent reaction selectivity towards all classes of hydrocarbons present in automotive fuels. No reaction is observed for common constituents of gasoline such as benzene, toluene, 1-pentene, 1-hexene, 2-methyl butane, butyraldehyde, and 2-methyl pentane at 453 K in binary or ternary mixtures with ethanol. All of these non-target hydrocarbons except butyraldehyde also have no impact on the ethanol partial oxidation rate or selectivity. MTBE proves to be active at 453 K over both $8VO_x/Al_2O_3$ and $Fe_2(MoO_4)_3$–MoO_3. Both MTBE and butyraldehyde decrease the ethanol reaction rate due to competitive surface adsorption on active sites but have no impact on the selectivity of the ethanol partial oxidation reaction.

1. Introduction

Recent emphasis on the use of ethanol as the primary oxygenate in automotive fuel has energized a demand for microsensors capable of pre- and post-engine analysis of ethanol content in complex volatile organic compound (VOC) mixtures [1]. Current VOC microsensor technologies are capable of only handling nonselective applications and are not adaptable for the analysis of ethanol in complex hydrocarbon mixtures including automotive fuels. Arrays comprised of 100 s of microsensors must be used to generate any degree of specificity in order to handle VOC mixtures of the complexity seen in automotive applications [2–4]; however, the use of microsensor arrays brings the disadvantages of higher power consumption and complex analytical programs, while still providing undesirable false positive responses [3].

New sensors will require the precision and accuracy of laboratory scale analytical tools, but at the same time must be inexpensive, low power, fast responding, and portable. Numerous classes of micro-gas sensor technologies are available and fabricated using MEMS or microsystem techniques, including semiconductor, dielectric, catalytic, resonance, and electrochemical sensors that transduce resistance, capacitance, temperature, or mass changes, among others [5,6]. However, all such microsensors are limited by their ability to sufficiently detect a specific analyte in complex multi-component gas mixtures [5–8]. Chemical specificity is the key bottleneck in the design of micro-gas sensors [5].

The sensing schematic explored in this work centers on addressing the issue of VOC selectivity without utilizing complex sensor arrays to accomplish such a goal. It builds upon the concept of a catalytic sensor by introducing a reactant selective catalyst to uniquely oxidize only the target VOC while allowing all other non-target VOCs to pass by it without generating a response. Commercially available catalytic microsensors use catalysts and conditions where all VOCs are unselectively oxidized [9]. In the new sensor scheme presented (Fig. 1), reaction and quantification of the target VOC will come via the placement of a selective catalyst on top of a microcalorimetric sensor. Temperature changes resulting from an isolated ethanol partial oxidation event can be transduced on chip into a quantitative measurement of ethanol concentration.

The challenge addressed in this work is the choice of a catalyst that oxidizes ethanol selectively in the presence of various classes of hydrocarbons representative of those present in automotive fuel. This can take the form of either selective adsorption and reaction of the target VOC in question or in the case where multiple species

* Corresponding author. Tel.: +1 765 496 7826; fax: +1 765 494 0805.
E-mail address: baertsch@purdue.edu (C.D. Baertsch).

0926-3373/$ – see front matter © 2010 Elsevier B.V. All rights reserved.
doi:10.1016/j.apcatb.2010.06.009

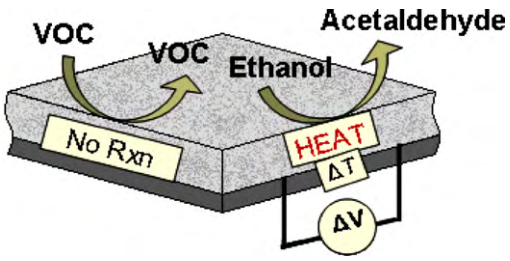

Fig. 1. Selective catalytic sensor schematic.

are active, by operating at a temperature at which the reaction rate of the target VOC is significantly higher than that of the non-target VOCs. On top of reactant selectivity, it is critical that the sensing catalyst provides the highest ethanol oxidation rate/gram possible as the sensitivity of such a sensor is directly tied to the amount of energy released due to reaction. Catalytic oxidation of ethanol to CO_2 is highly exothermic and favorable for maximum sensor sensitivity; however, this reaction typically occurs at temperatures where other hydrocarbons are also active for oxidation reactions [10]. A strong candidate explored in this paper is the partial oxidation of ethanol to acetaldehyde. This reaction pathway provides a significant heat of reaction while occurring at low temperatures over several metal oxide catalysts, thus minimizing the chance of undesirable side reactions involving non-target VOCs.

Metal oxide catalysts, specifically those containing dispersed vanadium and molybdenum oxides have a long history of catalytic reactions involving hydrocarbons [11–14]. Studies have shown that these oxides provide selectivity for reactions converting methanol to formaldehyde with selectivity as high as 96% at low conversions for temperatures under 573 K [11]. Another candidate is iron molybdate, which is a commercial catalyst for the production of formaldehyde from methanol. This catalyst exhibits formaldehyde yields as high as 95% and conversions approaching 100% at reaction temperatures under 673 K [12–15].

This work explores the application of vanadium and molybdenum oxides as selective catalysts for the detection of ethanol in complex hydrocarbon mixtures when coupled with a microcalorimetric sensor. A particular focus is on the impact of non-target VOCs on the rates and selectivity of the ethanol oxidative dehydrogenation reaction in order to investigate the impact on ethanol quantification. Gas mixtures studied are limited to binary and ternary mixtures of representative hydrocarbons present in automotive fuel in order to identify classes of compounds against which ethanol can be detected. Diffuse Reflectance Infrared Fourier Transform Spectroscopy (DRIFTS) studies and temperature programmed desorption were used to study the surface species present during reaction. These studies highlight that both selective adsorption and temperature can be used to achieve high reactant selectivity for target VOCs.

2. Experimental

2.1. Catalyst preparation

Supported metal oxide catalysts for this study were prepared by incipient wetness impregnation of γ-Al_2O_3 (Alcoa, HiQ® 7214F, surface area 151 $m^2\,g^{-1}$, pore volume 0.50 $cm^3\,g^{-1}$) with aqueous solutions of ammonium metavanadate (NH_4VO_3, Aldrich). Catalysts with vanadium surface densities ranging from 2 to 8 V-atoms/nm^2 were prepared. Oxalic acid at an oxalic acid/metal oxide salt weight ratio up to 1:1 was used to increase precursor solubility at higher metal oxide loadings. Metal atom surface densities are based on the initial alumina surface area available for impregnation (151 $m^2\,g^{-1}$). BET results obtained by N_2 physisorption at 77 K on a Micromeretics ASAP 2000 confirm that the surface area does not decrease significantly with impregnation as has been shown previously [16]. The impregnated samples where dried overnight at 393 K and then calcined in dry air (zero grade, 4.2 cm^3/s) at 923 K for 3 h.

Iron molybdate catalysts were co-precipitated from aqueous solutions of 2.3 M $Fe(NO_3)_3{\cdot}9H_2O$ and 0.3 M $(NH_4)_6Mo_7O_{24}{\cdot}4H_2O$ such that the volumes mixed in all samples prepared contained 2.0 Mo/Fe following a previously described procedure [17]. The ammonia heptamolybdate solution was initially chilled using an ice bath to 281 K. 100 mL of iron nitrate solution was then added to 100 mL ammonia heptamolybdate solution under vigorous stirring. After all of the iron nitrate solution was added, the temperature of the mixture was gradually increased to 287 K and held at this temperature for 20 min. The mixture was then heated to 303 K and aged for 2 h. At this point a dark green homogenous gel is formed. The sample was then dried at 343 K for 48 h in an oven, resulting in a reddish gel. This gel was dried at 453 K for 36 h to yield an orange powder. Catalyst powder was crushed to a particle size of <250 μm and calcined in dry air (zero grade, 4.2 cm^3/s) at 673 K for 4 h, resulting in a dark green solid.

2.2. Catalyst characterization

Bulk elemental compositions for all iron molybdate catalysts were determined by atomic absorption (AA) using a Perkin-Elmer Analyst 300 Spectrometer. Catalysts were dissolved in 3 M NH_4OH (~2.5 mL/mg catalyst for 30 min) and then diluted with distilled water. Concentrated HCl (5 M) was added (~5 mL/mg catalyst) to completely dissolve the samples [18]. Iron and molybdenum standards of 1, 5, and 10 mg/L were prepared from a 1000 mg/L standard solution (Ricca Chemical). Mo:Fe ratios were obtained from concentration measurements taken at a wavelength of 324.8 nm and a slit 0.7 nm.

Ultraviolet–visible (UV–vis) diffuse reflectance spectra (DRS) were obtained using a Varian (Cary 5000) spectrophotometer to characterize the domain size of supported vanadium oxide catalysts. Catalysts were ground to a fine powder and analyzed at ambient conditions. Data was collected by linear scanning in units of cm^{-1} over the range of 3500–50,000 cm^{-1}. Reflectance measurements (using MgO as a reflectance reference) were converted into pseudo-absorbance units using the Kubelka–Munk transform [19]. Edge energies were obtained by plotting $(F(R_\infty) * h\nu)^{1/2}$ vs $h\nu$ and extrapolating the linear region of the spectra around the absorption inflection point to the abscissa intercept [20,21].

Powder X-ray diffraction patterns of synthesized iron molybdate catalysts were recorded using a Scintag X2 Powder Diffractometer with Cu Kα radiation and a scanning rate of 1°/min. Raman spectroscopy was used to characterize the structure of synthesized iron molybdate catalysts. The Raman apparatus consists of a spectrograph SpectraPro 500i, holographic filter and TE-cooled Spec-10 Charged Coupled Device (CCD) (Roper Scientific) at 1340 × 400 pixels. A Notch filter (Kaiser Optical Systems) provides spectral edgewidth at 100 cm^{-1}. A 50 mW He–Ne laser was used as the excitation source at 632.8 nm. All samples were pretreated to 573 K for 1 h and cooled to room temperature. All Raman spectra were obtained at room temperature.

2.3. Ethanol partial oxidation reactions

Ethanol partial oxidation rates were measured using a continuous flow, fixed bed, U tube quartz reactor oriented vertically in a tube furnace. Temperature was measured using a thermocouple placed within a groove situated a couple of millimeters above

the catalyst bed which consisted of 15–100 mg of 125–250 μm catalyst particles. VO_x/Al_2O_3 and $Fe_2(MoO_4)_3$–MoO_3 catalysts were pretreated in 0.83 cm^3/s of simulated air (22% O_2 in He) at 773 K and 623 K, respectively, for 2 h in order to eliminate any moisture on the surface and to ensure complete oxidation.

Feed gases to the reactor consisted of 0.02–1.01 kPa ethanol and 1.52 kPa oxygen with the balance consisting of helium at 0.83–1.60 cm^3/s at 101.325 kPa total pressure and 453 K. For studies involving mixtures of hydrocarbons blended with ethanol, feed gases also included 0.02–1.01 kPa of each additional hydrocarbon. Ethanol (AAPER absolute 200 proof) was introduced into the feed as a liquid via a syringe pump (Cole-Palmer® 74900) and was vaporized into carrier gas at 353 K. Toluene (Alfa Aesar, anhydrous), benzene (Sigma–Aldrich, 99% thiophene free), 1-pentene (Alfa Aesar, >98%), n-hexane (Alfa Aesar, anhydrous), 1-hexene (Sigma–Aldrich, 99.8%), methyl-tert-butyl-ether (MTBE) (Alfa Aesar, HPLC grade), 2-methyl butane (Alfa Aesar, 99+%), 2-methyl pentane (Alfa Aesar, >99%), diethyl ether (Sigma–Aldrich, anhydrous >99.7%), and butyraldehyde (Sigma–Aldrich, 99%) were introduced in the same fashion. Reaction products were analyzed using an Agilent 6890 GC equipped with an HP-PLOT Q column with a thermal conductivity detector (TCD) and a flame ionization detector (FID). Conversion is reported as moles of ethanol reacted per moles of ethanol fed to the reactor. Molar selectivities are reported as moles of a particular product formed per moles of total products formed.

2.4. Catalyst surface studies

Temperature programmed desorption (TPD) measurements were conducted after pretreating 275 mg of VO_x/Al_2O_3 at a surface density of 8 V/nm^2 ($8VO_x/Al_2O_3$) in 0.83 cm^3/s of simulated air (22% O_2 in He) at 773 K for 3 h. Ethanol or toluene was adsorbed at 298 K. Upon surface saturation, helium was passed over the catalyst at room temperature to remove any weakly physisorbed species. Samples were heated at 10 K/min in 0.83 cm^3/s He. A Hiden Analytical Mass Spectrometer was used to monitor desorption of ethanol and toluene, monitoring intensities at m/e of 31 (ethanol), 44 (acetaldehyde), 59 (diethyl ether), and 91 (toluene) at a scanning rate of 5 scans/min to measure desorption rates as a function of temperature.

In situ diffuse reflectance infrared Fourier transform spectroscopy (DRIFTS) data was collected with a Nicolet Magna-860 spectrometer using a Harrick Scientific Praying Mantis diffuse reflectance accessory (DRA) and in situ reaction cell (HVC-DRP). Spectra were averaged over 128 scans with a resolution of 4 cm^{-1} and mirror velocity of 1.8988 cm s^{-1}. Approximately 0.030 g of powdered catalyst was loaded into the reaction cell and supported on a horizontal quartz frit. Gases were mixed upstream and passed downward through the catalyst bed. Temperature is measured and controlled by a thermocouple immediately beneath the catalyst bed. A background spectrum was collected at reaction temperature after pretreatment in 10% O_2 balance He at 773 K and used to convert reflectance measurements into pseudo-absorbance units. Powder catalysts were placed within the cell and pretreated in air at 573 K for 1 h. 0.5 kPa ethanol, 0.5 kPa toluene and 0.5 kPa butyraldehyde in 1.52 kPa O_2 with the balance consisting of helium at 0.83 cm^3/s at 101.325 kPa total pressure were delivered at 453 K for in situ studies.

3. Results and discussion

3.1. Structural characterization of VO_x/Al_2O_3 and $Fe_2(MoO_4)_3$

Edge energies determined from UV–vis absorbance spectra for supported vanadium oxide catalysts on alumina with surface densities ranging from 2 to 8 V/nm^2 were characterized (data not shown) and are consistent with trends and values reported in the literature [22], including the emergence of a second edge for catalysts with surface densities of 8 V/nm^2 and higher. Absorption edge energies decrease from 3.30 eV to 2.15 eV with increasing surface density from 0.5 to 8 V/nm^2 and characterize a systematic increase in VO_x domain size with increasing surface density up to the monolayer capacity of VO_x on alumina of ~8 V/nm^2 [23]. Upon reaching monolayer coverage, two edge energies are observed, indicating the simultaneous presence of both smaller 2-dimensional domains (E_0 at 2.40 eV) and V_2O_5 crystallites (E_0 at 2.15 eV).

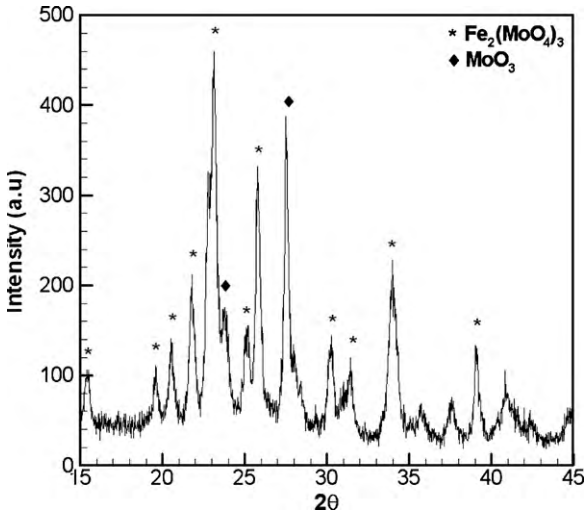

Fig. 2. X-ray diffraction (XRD) pattern for prepared $Fe_2(MoO_4)_3$–MoO_3.

X-ray diffraction was used to distinguish the crystalline phases present in prepared iron molybdate catalysts (Fig. 2). *D*-spacing calculations corresponding to interplanar spacing were found using Eq. (1):

$$n(\lambda) = 2d\sin(\theta) \quad (1)$$

where n is an integer, λ is the wavelength of the radiation, d is the interplanar spacing, and θ is the incident angle relative to the plane of atoms with the results shown in Table 1. Two of the most intense peaks located at D = 3.45 Å and D = 4.51 Å correspond with the MoO_3 phase [24]. Peaks corresponding to D-spacing values of D = 2.64 Å, 2.95 Å, 3.25 Å, 3.48 Å, and 3.84 Å correspond to the $Fe_2(MoO_4)_3$ phase [24]. Studies have shown that the selectivity and lifetime of the catalyst improves with the presence of excess molybdate. Commercial catalysts typically contain ratios as high as Mo/Fe = 5.0 (stoichiometric Mo/Fe in $Fe_2(MoO_4)_3$ = 1.5) [25–27].

The presence of excess MoO_3 was confirmed using Raman spectroscopy (Fig. 3). The MoO_3 phase is attributed to peaks located at 990 cm^{-1}, 810 cm^{-1} (asymmetric stretching Mo–O–Mo), 660 cm^{-1} (symmetric stretching in Mo–O–Mo), and 280 cm^{-1} (bending in terminal Mo=O), while peaks at 965 cm^{-1} (stretching in Mo=O), 930 cm^{-1} and 780 cm^{-1} (stretching of Mo–O–Mo) correspond to

Table 1
XRD *D*-spacing analysis for $Fe_3(MoO_4)_3$–MoO_3.

D (Å)	I/I_o (%)
3.84	100.0
3.23	84.2
3.45	62.1
2.63	49.4
4.07	40.0
3.72	37.1
4.32	30.6
2.95	30.1

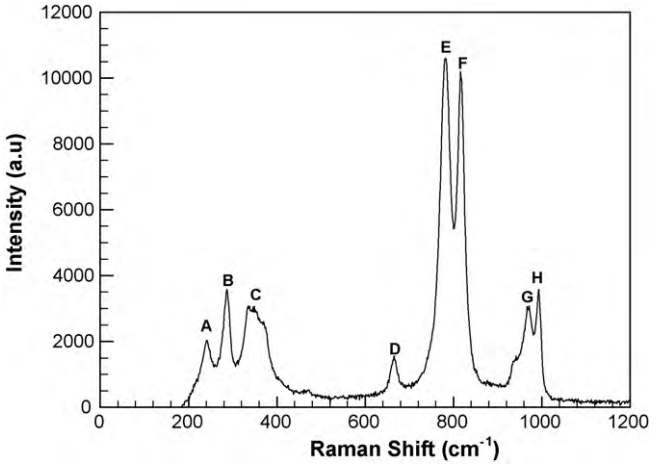

Fig. 3. Raman spectrum for prepared $Fe_2(MoO_4)_3$–MoO_3: (A) and (B) deformations of Mo–O–X, (C) bending in terminal Mo=O, (D) symmetric stretching of Mo–O–Mo in MoO_3, (E) stretching of Mo–O–Mo in $Fe_2(MoO_4)_3$, (F) stretching of Mo–O–Mo in MoO_3, (G) Mo=O in $Fe_2(MoO_4)_3$, (H) Mo=O in MoO_3 [18,29,30].

the $Fe_2(MoO_4)_3$ phase [18,28,29]. Raman spectroscopy results shown in Fig. 3 confirm the presence of both the $Fe_2(MoO_4)_3$ phase and the MoO_3 phase, indicating that the Mo/Fe ratio of the precipitated catalyst surpasses the stoichiometric requirement for $Fe_2(MoO_4)_3$ since no iron oxide phases were simultaneously observed. Atomic absorption analysis verifies that excess molybdenum is present, giving a Mo/Fe ratio of 1.9. Thus, throughout this manuscript, the prepared catalyst is denoted as $Fe_2(MoO_4)_3$–MoO_3.

3.2. Reactivity and selectivity of ethanol oxidative dehydrogenation

Oxidative reactions of ethanol were conducted over a series of VO_x/Al_2O_3 catalysts with different vanadium surface densities and over $Fe_2(MoO_4)_3$–MoO_3. Rates and selectivities at 453 K are reported in Table 2. None of the catalysts investigated deactivate during reaction with ethanol at this temperature and rates are stable for as long as reactions have ever been tested (more than 10 h), indicating that the surface area is also unaffected by reaction. Further, catalysts can be reoxidized in dry air at 773 K to obtain the same rate obtained on a different day, within experimental error (as reported in Table 3 and Fig. 4). Only a slight change in catalyst color is observed for higher surface density samples due to reduction in ethanol.

Ethanol reaction rates over VO_x/Al_2O_3 and $Fe_2(MoO_4)$–MoO_3 are independent of conversion over the conversion range investigated (<15%), as shown in Fig. 4. Acetaldehyde selectivity during ethanol oxidative dehydrogenation over alumina-supported vanadium oxide increases with increasing surface density (Table 2).

Table 2
Ethanol conversion rates and selectivities at 453 K over VO_x/Al_2O_3 and $Fe_2(MoO_4)_3$–MoO_3 (0.5 mol% ethanol, 1.5 mol% O_2, 15.0–80 mg catalyst, with ethanol conversions 2–12%).

Catalyst	Ethanol rate (mol/g s × 10^{-6})	Acetaldehyde selectivity (%)	Diethyl ether selectivity (%)
MoO_3	0.06	73.8	26.2
V_2O_5	0.46	94.5	5.5
$Fe_2(MoO_4)_3$	3.4	99.3	0.7
$8VO_x/Al_2O_3$	1.3	94.2	5.4
$6VO_x/Al_2O_3$	1.6	89.1	10.9
$4VO_x/Al_2O_3$	1.3	80.0	20.0
$2VO_x/Al_2O_3$	0.67	74.8	25.2
$0.5VO_x/Al_2O_3$	0.94	31.8	68.2

Table 3
Effect of ethanol concentration on ethanol conversion rate as a function of concentration over $8VO_x/Al_2O_3$ and $Fe_2(MoO_4)_3$ (1.5 mol% O_2, 453 K, conversions < 10%). Error represents a 95% confidence interval.

Catalyst	Ethanol feed concentration (mol%)	Rate (mol ethanol reacted/m2 s)
$8VO_x/Al_2O_3$	0.50	$8.4 \pm 0.2 \times 10^{-9}$
	0.25	$8.6 \pm 0.2 \times 10^{-9}$
	0.20	$8.7 \pm 0.2 \times 10^{-9}$
$Fe_2(MoO_4)_3$	0.50	$3.4 \pm 0.2 \times 10^{-7}$
	1.00	$3.6 \pm 0.3 \times 10^{-7}$
	2.00	$3.7 \pm 0.2 \times 10^{-7}$

Once monolayer coverage is achieved on the alumina support (8 V/nm^2), the selectivity of 94.2% is nearly identical to that observed over bulk V_2O_5 (94.5%). The only other product is diethyl ether. Below monolayer coverage ether is produced on the exposed acidic alumina surface sites. Both monolayer VO_x/Al_2O_3 and $Fe_2(MoO_4)_3$–MoO_3 prove to be viable candidates for the selective catalytic detection of ethanol in vapor fuels since they provide high selectivity towards a single exothermic product, producing acetaldehyde with a vapor phase heat of reaction of −177.8 kJ/mol upon reaction at low temperature. It should be noted that the acid catalyzed reaction, producing diethyl ether at 453 K over these catalysts, is also exothermic (−26.1 kJ/mol). However, high selectivity to acetaldehyde is desirable because its larger reaction heat will enhance sensor sensitivity. Utilization of $Fe_2(MoO_4)_3$–MoO_3, rather than VO_x/Al_2O_3, will also increase sensor sensitivity because its higher rate per gram will yield more heat generation per gram of catalyst loaded onto a microsensor device.

While conversion rates per gram provide good comparisons of the utility of these catalysts in a microsensor device, such rates do not provide meaningful comparison between the functionality and site density between these two catalysts of interest. Areal rates per m^2 of surface area are given in Table 3 and show that either the density of active sites, the intrinsic conversion rate, or a combination of the two leads to a 100× increase in the rate per m^2 over $Fe_2(MoO_4)_3$–MoO_3 compared to monolayer VO_x/Al_2O_3. It should be noted that, over these oxide catalysts, acetaldehyde formation proceeds through a Mars-van Krevelen type redox mechanism where ethanol adsorbs as an ethoxy species on the surface and the rate determining step for acetaldehyde formation is the removal of an alpha hydrogen from carbon in the adsorbed ethoxy species to an active O* site, from which one oxygen from the catalyst surface is removed for each acetaldehyde produced in a mechanism which

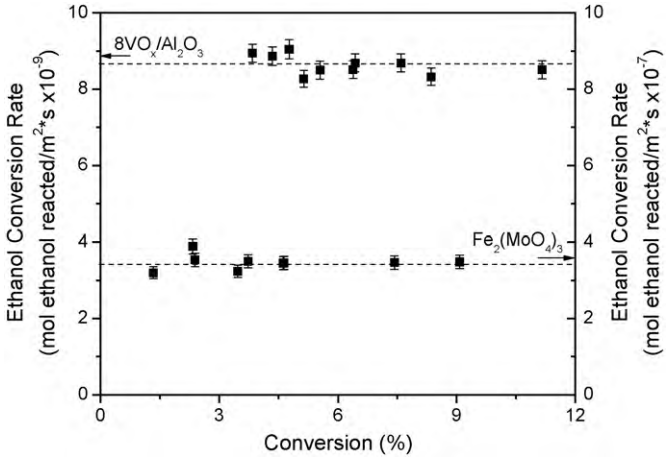

Fig. 4. Ethanol rate at 453 K as a function of conversion over $8VO_x/Al_2O_3$ and $Fe_2(MoO_4)_3$–MoO_3 (0.5 mol% ethanol, 1.5 mol% O_2, 2–50 mg catalyst). Error bars represent 95% confidence intervals.

Table 4
Product selectivity as a function of ethanol conversion over $8VO_x/Al_2O_3$ and $Fe_2(MoO_4)_3$ at 453 K (0.5 mol% ethanol, 1.5 mol% O_2, 15–150 mg of catalyst).

Catalyst	Ethanol conversion range (%)	Acetaldehyde selectivity (%)	Ether selectivity (%)	Acidic acid and ethyl acetate selectivity (%)
$8VO_x/Al_2O_3$	<10	94.6	5.4	–
	40–50	94.0	3.3	2.7
$Fe_2(MoO_4)_3$–MoO_3	<10	99.3	0.7	–
	30–45	98.0	0.6	1.4

parallels that of formaldehyde formation from methanol [30–32]. During steady state reaction, the catalyst is then reoxidized by gas-phase oxygen present in the reactant feed. Previous results have shown that intrinsic TOFs for ethanol oxidative dehydrogenation over MoO_x, VO_x, and WO_x catalysis supported on alumina at various metal atom surface densities are identical and centered around 1.0×10^{-3} s^{-1} at 453 K [33]. These comparable TOFs show that the determining factor for acetaldehyde formation rates over all of these metal oxide catalysts is the density of available redox sites in each catalyst. As such, it appears that the redox site density on $Fe_2(MoO_4)_3$–MoO_3 is much higher than on VO_x/Al_2O_3. An ideal catalyst for selective ethanol detection is one that maximizes the density of available redox sites in order to maximize conversion rates per gram and thus sensor sensitivity.

3.3. Requirements for ethanol quantification

For microcalorimetric detection of ethanol during reaction, a sensor signal will be dependent on the total amount of ethanol converted over the catalyst (i.e. the total heat produced). If the rate of ethanol oxidation is dependent on ethanol concentration then quantification can occur at any degree of conversion. If the rate of ethanol oxidation is independent of ethanol concentration (zero order), quantification must occur at complete conversion. The latter case would set limits on the maximum amount of ethanol that could be quantified and would be dependent on catalyst loading, residence time, and catalytic rate.

Ethanol oxidation rates were investigated as a function of ethanol concentration over both the $8VO_x/Al_2O_3$ and $Fe_2(MoO_4)_3$–MoO_3 catalysts at 453 K. At this temperature, the surface is saturated with ethoxy species at 453 K. In situ DRIFTS spectra show no change in ethoxy coverage with ethanol concentration (>0.05 kPa ethanol partial pressures). As a result, ethanol conversion rates are not dependent on ethanol concentration (Table 3). Thus, quantification of ethanol in a calorimetric sensor using either of these catalysts as a substrate would require operation at complete conversion.

Since the sensor must operate at complete conversion for quantification purposes, the selectivity of VO_x/Al_2O_3 and $Fe_2(MoO_4)_3$–MoO_3 catalysts at high conversion at 453 K were investigated. As shown in Table 4, the product selectivity does not change significantly at higher conversion. Selectivity is independent of conversion over these catalysts at 453 K because acetaldehyde and diethyl ether appear to be primary products formed via parallel reactions from adsorbed ethoxy species; readsorption and subsequent reaction of these products does not occur.

3.4. Ethanol reactivity in mixtures with alkanes, alkenes, and aromatics

In order for a catalytic sensor to provide a chemically specific and selective response corresponding to ethanol, all other components in the sample gas mixture must be inert under operating conditions (or provide very low tolerable reaction heats). To test the feasibility of converting ethanol to acetaldehyde selectively in the presence of other hydrocarbons, particularly those present in automotive fuel and post-engine streams, the reactivity of equimolar binary and tertiary mixtures was investigated containing ethanol with benzene, toluene, 1-pentene, methane, n-hexane, 1-hexene, 2-methyl propane, 2-methyl butane, diethyl ether, butyraldehyde, and methyl-tert-butyl-ether (MTBE). All of these hydrocarbons proved to be inactive over both $8VO_x/Al_2O_3$ and $Fe_2(MoO_4)_2$–MoO_3 at 453 K except for MTBE which exhibited substantial activity and is discussed in Section 3.5.

In addition to having a very low rate compared to ethanol, it is important that other non-target gas species do not influence the ethanol reaction rate and/or selectivity, even if these species themselves do not undergo reaction, so that calibrations of the thermal response from the ethanol reactions can be applied to analysis in any gas mixture. Ethanol conversion rates and product selectivities in equimolar binary and tertiary mixtures with inactive hydrocarbons are shown in Figs. 5 and 6 for $8VO_x/Al_2O_3$ and $Fe_2(MoO_4)_3$–MoO_3, respectively. Benzene, toluene, 1-pentene, methane, n-hexane, 1-hexene, 2-methyl propane, and 2-methyl butane have no impact on the rate and selectivity of ethanol partial oxidation over either catalyst in question. Thus, ethoxy surface coverages and active redox sites are unchanged in these mixtures.

The relative concentration of ethanol to other hydrocarbons in gasoline can vary greatly, as seen in available E10 (total hydrocarbons to ethanol 9:1; aromatics to ethanol ~3:1) and E85 fuels (total hydrocarbons to ethanol 15:85, aromatics to ethanol 5:85) [34]. Ethanol/toluene binary mixtures over $8VO_x/Al_2O_3$ were used as a case study to investigate the effect of hydrocarbon ratio on ethanol reaction rate and selectivity since aromatics represent one of the largest fractions of hydrocarbons in fuel. As seen in Table 5, neither the ethanol rate nor acetaldehyde selectivity changes with different ethanol/toluene ratios. This indicates that even in the worse case scenarios of significantly higher aromatic content, ethanol oxidative dehydrogenation rates and selectivity are not affected by their presence, assuring that detection should be possible across the breath of aromatic concentrations present in automotive fuel.

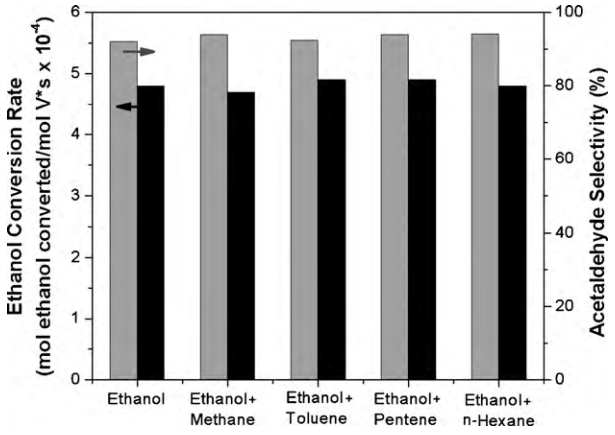

Fig. 5. Ethanol conversion rate and acetaldehyde selectivity at 453 K over $8VO_x/Al_2O_3$. (▒) Acetaldehyde selectivity (%), (■) ethanol rate. Run conditions: 0.5% ethanol, 0.5% n-hexane, 0.5% toluene, 1.5% methane, 1.5% O_2, 453 K, ~25.0 mg $8VO_x/Al_2O_3$ at 2–10% conversion.

Table 5
Ethanol activity at 453 K upon toluene addition over $8VO_x/Al_2O_3$ (0.5 mol% ethanol, 0–2 mol% toluene, 1.5 mol% O_2, balance He).

Reactants	Molar ratio (EtOH:toluene)	Ethanol rate (mol EtOH/mol V s × 10^{-4})	Acetaldehyde selectivity (%)	Diethyl ether selectivity (%)
Ethanol	∞	4.8 ± 0.2	94.6	5.4
Ethanol:toluene	(1:2)	4.8 ± 0.2	94.9	5.1
Ethanol:toluene	(1:4)	4.6 ± 0.2	94.7	5.3

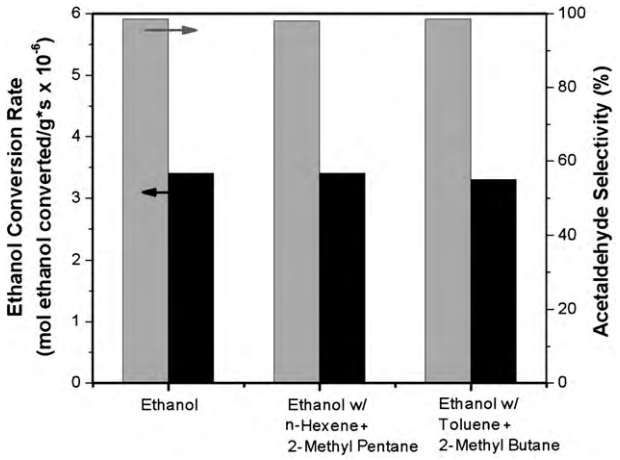

Fig. 6. Ethanol conversion rate and acetaldehyde selectivity at 453 K over $Fe_2(MoO_4)_3$–MoO_3. (■) Acetaldehyde selectivity (%), (■) ethanol rate. Run conditions: 0.5% ethanol, 0.5% n-hexane, 0.5% toluene, 0.5% 2-methyl pentane, 0.5% 2-methyl butane, 1.5% O_2, 453 K, ~18.0 mg $Fe_2(MoO_4)_3$ at 2–10% conversion.

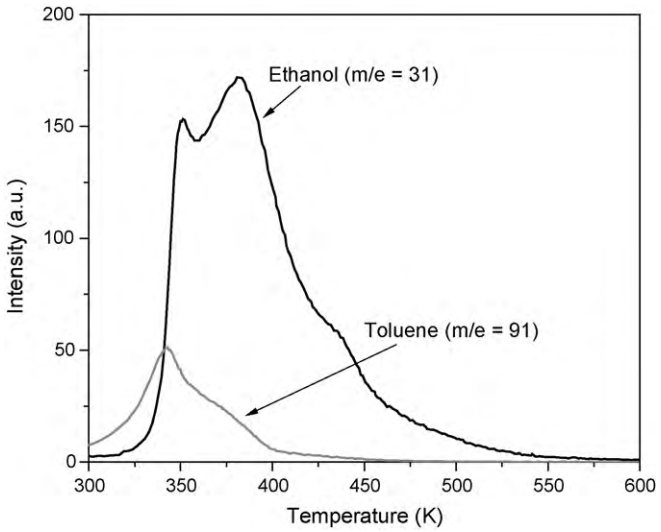

Fig. 7. Temperature programmed desorption of ethanol and toluene over $8VO_x/Al_2O_3$ (adsorption at 398 K in He; desorption in He at 0.17 K s^{-1}).

These combined results indicate that ethanol quantification in mixtures involving a wide range of non-active hydrocarbon classes (parafins, olefins, and aromatics) are possible using both $8VO_x/Al_2O_3$ and $Fe_2(MoO_4)_3$–MoO_3. These non-active, non-target hydrocarbons do not interfere with ethanol reactions because they are not present on the catalyst surface at the proposed sensing temperature of 453 K. Temperature programmed desorption results (Fig. 7) show that all toluene adsorbed at room temperature desorbs at temperatures below 453 K, whereas more than 8% of the ethanol adsorbed at room temperature remains on the surface at 453 K.

DRIFTS studies of ethanol and ethanol/toluene mixtures over $8VO_x/Al_2O_3$ were conducted in order to study the surface species

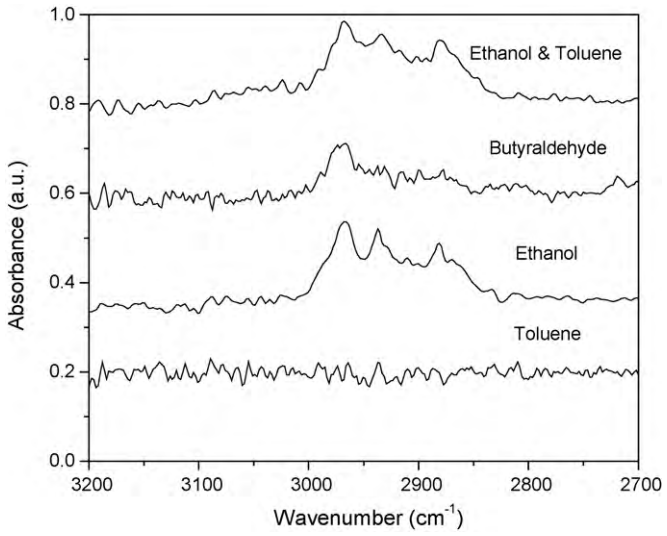

Fig. 8. In situ DRIFTS spectra for ethanol, toluene, butyraldehyde, and an ethanol/toluene mixture over $8VO_x/Al_2O_3$ at 453 K. Run conditions: 0.5% ethanol, 0.5% toluene, 0.5% butyraldehyde, 1.5% O_2, ~50.0 mg $8VO_x/Al_2O_3$.

present under reaction conditions. As seen in Fig. 8, peaks associated with the formation of ethoxy species on the surface are located at 2880 cm^{-1} and 2900 cm^{-1}, resultant from the stretching node, $\nu(CH_2)$, while peaks located at 2970 cm^{-1} and 2940 cm^{-1} are associated with $\nu_{as}(CH_3)$ and $\nu(CH_3)$, respectively [35]. The introduction of 0.5 kPa toluene at 453 K results in no adsorbed surface species. When an equimolar mixture of 0.5 kPa toluene and 0.5 kPa ethanol is introduced at 453 K, the intensities of peaks associated with ethoxy species cannot be differentiated from those present during reaction with pure ethanol, and no additional peaks associated with adsorbed toluene species are present. Thus, toluene does not adsorb on the surface of the catalyst at 453 K; the presence of toluene impacts neither the ethoxy surface concentration nor the ethanol conversion rate.

3.5. Ethanol reactivity in mixtures with ethers and aldehydes

MTBE exhibits significant activity at 453 K over both catalysts. In fact, MTBE is converted over both of these metal oxide catalysts at temperatures as low as 343 K with the rate and selectivity shown in Table 6. Over both $8VO_x/Al_2O_3$ and $Fe_2(MoO_4)_3$–MoO_3, MTBE follows an acid catalyzed pathway producing isobutene and methanol. The magnitude of this rate paired with its significant heat of reaction (62.1 kJ/mol) would result in false positive responses over both of these catalysts at 453 K while convoluting the ethanol rate and thermal signature.

Unlike the aromatics, parafins, and olefins tested, the presence of MTBE, diethyl ether and butyraldehyde decreases ethanol oxidative dehydrogenation rates over both $8VO_x/Al_2O_3$ and $Fe_2(MoO_4)_3$–MoO_3 (Figs. 9 and 10). The presence of butyraldehyde on the surface of $8VO_x/Al_2O_3$ at 453 K is verified by DRIFTS as seen in Fig. 8; ethanol rates are reduced due to competitive adsorption on metal sites. Neither the addition of MTBE, diethyl ether, nor butyraldehyde affects ethanol reaction selectivity (Figs. 9 and 10),

Table 6
MTBE reaction rates over $8VO_x/Al_2O_3$ and $Fe_2(MoO_4)_3$–MoO_3 at 343 K (1.0 mol% MTBE, 3.0 mol% O_2, bal He).

Catalyst	MTBE reaction rate (mol MTBE reacted/g s × 10^{-7})	Methanol selectivity (%)	Isobutene selectivity (%)
$8VO_x/Al_2O_3$	37.0	50.0	50.0
$Fe_2(MoO_4)_3$	9.5	50.0	50.0

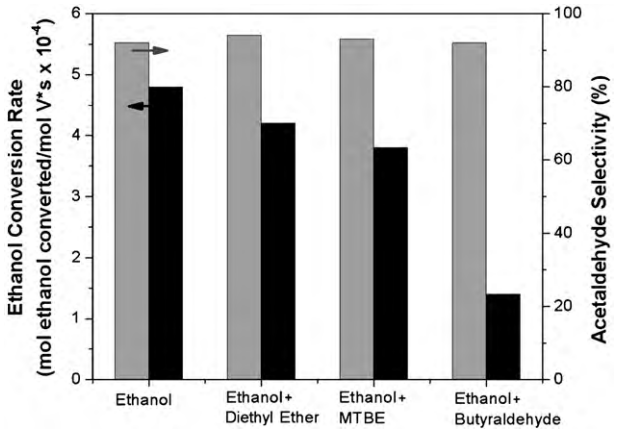

Fig. 9. Ethanol conversion rate and acetaldehyde selectivity at 453 K over $8VO_x/Al_2O_3$. (▒) Acetaldehyde selectivity (%), (■) ethanol rate. Run conditions: 0.5% ethanol, 0.5% diethyl ether, 0.5% MTBE, 1.5% butyraldehyde, 1.5% O_2, ~25.0 mg $8VO_x/Al_2O_3$, 2–10% conversion.

indicating that a universal ethoxy species leads to both ether and aldehyde production.

As previously discussed, detection of ethanol using either of these catalysts coupled with a thermal sensor is restricted to operating at conditions where all of the ethanol entering the sensor reactor is converted to acetaldehyde since ethanol oxidative dehydrogenation rates are independent of ethanol concentration. Although hydrocarbon components such as butyraldehyde will not lead to the generation of false positive results on the sensor (they are unreactive at 453 K), competitive adsorption affects that diminish ethanol rates will also diminish the ranges of concentrations that can be completely converted for a given catalyst weight and residence time through the sensor.

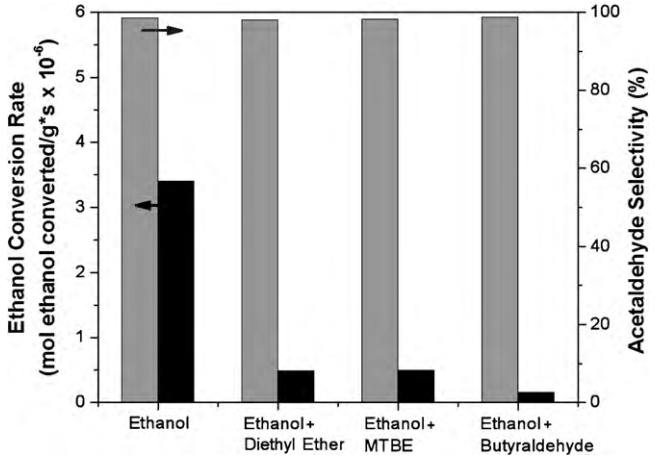

Fig. 10. Ethanol conversion rate and acetaldehyde selectivity at 453 K over $Fe_2(MoO_4)_3$–MoO_3. (▒) Acetaldehyde selectivity (%), (■) ethanol rate. Run conditions: 0.5% ethanol, 0.5% diethyl ether, 0.5% MTBE, 0.5% butyraldehyde, 1.5% O_2, ~18.0 mg $Fe_2(MoO_4)_3$, 2–10% conversion.

4. Conclusions

Selective reaction of ethanol in mixtures involving many of the hydrocarbons present in fuel is shown to be possible using either $8VO_x/Al_2O_3$ or $Fe_2(MoO_4)_3$–MoO_3 as the active catalyst coupled with a microthermal gas sensor. Both catalysts meet the requirements of promoting the oxidative dehydrogenation of ethanol to acetaldehyde at low temperatures with nearly 100% selectivity. Comparing the two, $Fe_2(MoO_4)_3$–MoO_3 provides a higher acetaldehyde production rate on a per gram basis and thus would provide higher sensitivity to ethanol than the $8VO_x/Al_2O_3$ catalyst for a similar weight loading. $Fe_2(MoO_4)_3$–MoO_3 has a higher areal rate than $8VO_x/Al_2O_3$, presumably due to a larger redox site density. Both catalysts exhibit rates that are independent of ethanol concentration across the ranges tested indicating that quantification can only occur when operating under complete conversion.

$Fe_2(MoO_4)_3$–MoO_3 or $8VO_x/Al_2O_3$ are both sufficient catalyst selections to couple with a microthermal sensor for selective ethanol quantification in many hydrocarbon mixtures, including those containing: benzene, toluene, 1-pentene, methane, n-hexane, 1-hexene, 2-methyl propane, and 2-methyl butane. Both $Fe_2(MoO_4)_3$–MoO_3 and $8VO_x/Al_2O_3$ are able to uniquely oxidize ethanol while allowing a majority of other non-target VOCs to pass through a sensor without generating a response. This provides a significant improvement in microsensor technology by introducing chemical specificity in complex hydrocarbon mixtures without utilizing large microsensor arrays. However, the same approach using a single catalytic sensor is not viable for ethanol detection in mixtures containing ethers and aldehydes, including diethyl ether, butyraldehyde, and MTBE. These non-target hydrocarbons decrease ethanol oxidative dehydrogenation rates over both $8VO_x/Al_2O_3$ and $Fe_2(MoO_4)_3$–MoO_3 due to competitive adsorption effects. In addition, MTBE proves to be significantly active at 453 K and would further convolute the thermal signal.

Acknowledgements

This work, including graduate student support for J.E. Gatt, was provided by NSF (CBET Career Award #0644707) and Purdue University. H. Nair was supported by the Bilsland Dissertation Fellowship at Purdue University.

References

[1] H. Svenningstorp, B. Widen, P. Salomonsson, L.G. Ekedahl, I. Lundstrom, P. Tobias, A.L. Spetz, Sens. Actuators B 77 (1–2) (2001) 177–185.
[2] S.D. Choi, D. Lee, Sens. Actuators B 77 (2001) 335–338.
[3] D.S. Lee, J.K. Jung, J.W. Lim, J.S. Huh, D.D. Lee, Sens. Actuators B 77 (1–2) (2001) 228–236.
[4] P. Lv, Z. Tang, G.F. Wei, J. Yu, Z.X. Huang, Meas. Sci. Technol. 18 (2007) 2997–3004.
[5] T. Simon, N. Barsan, M. Bauer, U. Weimar, Sens. Actuators B 73 (1) (2001) 1–26.
[6] W. Goepel, K.D. Schierbaum, Sens. Actuators B 26 (1995) 1–12.
[7] J.S. Suehle, R.E. Cavicchi, M. Gaitan, S. Semancik, IEEE Electron Device Lett. 14 (3) (1993) 118–120.
[8] C. Hagleitner, A. Hierlemann, D. Lange, A. Kummer, N. Kerness, O. Brand, H. Baltes, Nature 414 (2001) 293–296.
[9] J. Janata, A. Bezegh, Anal. Chem. 60 (12) (1988) 62–72.
[10] G. Avgouropoulos, E. Oikonomopoulos, D. Kanistras, T. Ioannides, Appl. Catal. B 65 (2006) 62–69.
[11] L. Briand, L. Gambaro, H. Thomas, J. Catal. 161 (2) (1996) 839–860.
[12] M.D. Argyle, K.D. Chen, A.T. Bell, E. Iglesia, J. Catal. 208 (1) (2002) 139–149.
[13] M. Cherian, M.S. Rao, G. Deo, Catal. Today 78 (1–4) (2003) 397–409.

[14] S.H. Taylor, J.S.J. Hargreaves, G.J. Hutchings, R.W. Joyner, C.W. Lembacher, Catal. Today 42 (3) (1998) 217–224.
[15] G.D. Kolovertnov, G.K. Boreskov, V.A. Dzisko, B.I. Popov, D.V. Tarasova, G.C. Belugina, Kinet. Catal. (Engl. Transl.) 6 (6) (1965) 950.
[16] D.R. Milburn, B.D. Adkins, B.H. Davis, Appl. Catal. A 119 (1994) 205.
[17] P. Courty, US Appl. #3,846,341, 5 November, 1974.
[18] C.G. Hill, J.H. Wilson, J. Mol. Catal. 63 (1) (1990) 65–94.
[19] E.L. Simmons, Appl. Opt. 14 (1975) 1380.
[20] P. Kubelka, F. Munk, Z. Tech. Phys. 12 (1931) 593.
[21] R.A. Smith, Semiconductors, 1978.
[22] M.D. Argyle, K. Chen, A.T. Bell, E. Iglesia, J. Catal. 208 (2002) 193.
[23] H.X. Dai, A.T. Bell, E. Iglesia, J. Catal. 221 (2004) 491–499.
[24] A.P.V. Soares, M.F. Portela, A. Kiennemann, Stud. Surf. Sci. Catal. 110 (1997) 807.
[25] N. Pernicone, J. Less-Common Met. 36 (1974) 289.
[26] I. De La Torre, G. Acosta, Rev. Inst. Mex. Petról 11 (4) (1979) 68.
[27] A.B. Stiles, T.A. Koch, M. Dekker (Eds.), Oxidation Catalysts in Catalyst manufacture, 2nd ed., 1995, New York, chapter 20.
[28] P.L. Villa, A. Szabo, F. Trifirò, M. Carbucicchio, J. Catal. 47 (1997) 122.
[29] P. Forzatti, P.L. Villa, N. Ferlazzo, D. Jones, J. Catal. 76 (1982) 188.
[30] W. Zhang, S.T. Oyama, J. Phys. Chem. 100 (1996) 10759.
[31] W.E. Farmeth, E.M. McCarron, A.W. Sleight, R.H. Staley, Langmuir 3 (1987) 217.
[32] W.E. Farmeth, R.H. Staley, A.W. Sleight, J. Am. Chem. Soc. 109 (1986) 2329.
[33] H. Nair, C.D. Baertsch, J. Catal. 258 (2008) 1–4.
[34] C. Huang, L. Wei, L.B. Yang, J. Wang, Y. Li, L. Sheng, Y. Zhang, F. Qi, Energy Fuels 20 (2006) 1505.
[35] S.T. Oyama, W. Zhang, J. Am. Chem. Soc. 118 (1996) 7173.